Cement and Concrete Research 125 (2019) 105858

Contents lists available at ScienceDirect

Cement and Concrete Research

journal homepage: www.elsevier.com/locate/cemconres

Conceptual design and performance evaluation of two-stage ultra-low binder ultra-high performance concrete

P.P. Li[a,b], Q.L. Yu[b,c,*], H.J.H. Brouwers[a,b], W. Chen[a,**]

[a] State Key Laboratory of Silicate Materials for Architectures, Wuhan University of Technology, Wuhan 430070, PR China
[b] Department of the Built Environment, Eindhoven University of Technology, P.O. Box 513, 5600 MB Eindhoven, the Netherlands
[c] School of Civil Engineering, Wuhan University, 430072 Wuhan, PR China

ARTICLE INFO

Keywords:
Two stage ultra-high performance concrete
Compatibility
ITZ
Binder efficiency
Prediction model

ABSTRACT

This study proposes a novel concept of two-stage ultra-high performance concrete (TS-UHPC), towards ultra-low binder consumption. The effects of grout and coarse aggregate are investigated and their compatibility is evaluated. Results show that TS-UHPC has a low binder amount (down to 364 kg/m^3) and high binder efficiency (up to 0.417 MPa·m^3/kg), possessing excellent compressive strength of up to 151.8 MPa at 91 days. Microstructural analysis reveals that grout with a sand-to-powder ratio of 1.0 shows a higher hydration degree, denser structure, and increased later strength. Coarser basalt aggregate tends to slightly lower compressive and splitting tensile strength, 14% and 12% reduction with the maximum size from 8 mm to 25 mm, respectively. The TS-UHPC has an excellent interfacial transition zone that induces a water-permeable porosity of 0.91%–1.32%. New formulas are proposed to describe correlation between compressive and splitting tensile strength of TS-UHPC, and to predict strength of TS-UHPC by grout.

1. Introduction

Ultra-high performance concrete (UHPC) is an advanced building material with wide application potentials, attributed to its superior workability, mechanical property, impact resistance and durability [1–4]. One of the key mix design principles is to eliminate coarse aggregate and utilize large amount binder to increase homogeneity of UHPC and overcome inherent weakness of interfacial transition zone (ITZ) [5–7], usually more than 900 kg/m^3 binders are consumed [8]. It causes some disadvantages, such as poor economic benefit and sustainability issue, large autogenous shrinkage, and thermal induced cracks in mass concrete.

Introducing appropriate coarse aggregates into UHPC is a promising attempt to solve the above mentioned problems. The utilization of coarse aggregates in conventional concrete has apparent advantages, such as reduced autogenous shrinkage [2], improved elastic modulus and workability [9], enhanced stress-strain behaviour of confined concrete [10], strengthened impact resistance under high velocity projectile [11]. In recent years, researchers have attempted to incorporate coarse aggregates into UHPC and acquired good results. Our previous research showed that coarse basalt aggregates have negligible negative effect on the mechanical strength, with a significantly reduced powder amount of UHPC [12], and improved low-velocity impact resistance [13]. Pyo et al. [14,15] produced UHPC incorporating coarser aggregates with maximum particle size of 5.2 mm, and revealed excellent abrasion resistance, strain hardening behaviour and a limited decrease in tensile strength. Liu et al. [16] designed UHPC combined with coarse aggregates (5–20 mm) and fibres, and found that coarse aggregates could be successfully introduced into the system of UHPC without impairing tensile properties at a favourable replacement level (25% by the volume of UHPC matrix). Wu et al. [17,18] investigated the projectile impact resistance of basalt or corundum aggregated UHPC, proved that enlarging the size of the coarse aggregates could help to reduce the penetration depth, impact crater area and volume. However, those attempts only use limited volume replacement levels (e.g. 25% by the volume of UHPC matrix in Ref. [17]) and maximum particle sizes (e.g. 5.2 mm in Ref. [15]) of coarse aggregates, and the powder contents are still quite large (e.g. 770–1100 kg/m^3 in Ref. [18]). Besides, coarse aggregates with low density and strength are not compatible with the relatively high strength of UHPC matrix. While high strength coarse aggregates usually have dense structure and high density, which more easily causes segregation problem in UHPC system. Hence, how to further increase the volume and size of coarse aggregate and reduce the binder consumption in UHPC system is still an issue and

* Correspondence to: Q.L. Yu, Department of the Built Environment, Eindhoven University of Technology, P.O. Box 513, 5600 MB Eindhoven, the Netherlands.
** Corresponding author.
E-mail addresses: q.yu@bwk.tue.nl (Q.L. Yu), chen.wei@whut.edu.cn (W. Chen).

https://doi.org/10.1016/j.cemconres.2019.105858
Received 6 February 2019; Received in revised form 5 August 2019; Accepted 6 August 2019

potential research subject.

Two-stage (preplaced aggregate) concrete (TSC) is an effective way to extend the utilization of coarse aggregates, which is produced by first preplacing aggregates in a formwork and subsequently injecting grout [19,20]. High volumes of large size aggregates can be easily used, due to its fabrication methodology without any segregation concerns [20]. A higher volume (e.g. 53%–59% in Ref. [19, 21]) means a much lower binder consumption. A larger maximum particle size of the aggregates (e.g. 40 mm in Ref. [22]) indicates a better resistance against bullet or projectile impact [18]. TSC has already been successfully used in applications including underwater concrete construction, massive concrete structure, casting concrete in areas with narrowly spaced reinforcement, concrete repair, heavyweight concrete and low-shrinkage concrete. Nevertheless, the strength of current TSC is relatively low, usually ranging between 10 MPa to 60 MPa [19–25], which is probably attributed to low intrinsic strength of coarse aggregates, relatively low strength of the grout, weak homogeneity, stress concentration at the contact points between aggregates, inherent weakness between coarse aggregate and paste matrix. To sum up, UHPC and TSC have some complementary characteristics on coarse aggregate utilization, binder consumption and mechanical properties. Hence, there is potential to design a novel building material to make full use of advantages of TSC and UHPC and overcome their individual shortages.

This paper aims to develop two-stage ultra-high performance concrete (TS-UHPC) as a novel building material, including fabrication methodology, excellent mechanical properties, high volume coarse aggregate and very low binder consumption, possessing widely potential application, e.g. impact resistant, underwater, massive, repaired, heavyweight, low-shrinkage and narrowly spaced reinforced concrete. The properties of grouts are assessed by fresh behaviour, hydration kinetics, pore structure and compressive strength. The mechanical behaviour of TS-UHPC is evaluated in terms of compressive and splitting tensile strength, as well as binder efficiency. The compatibility between grout and aggregate is analysed by assessing the interfacial transition zone (ITZ). New models are proposed and validated to correlate the compressive strength and tensile splitting strength of TS-UHPC, and compressive strength of TS-UHPC and grout. The proposed TS-UHPC concept further contributes to sustainability development of advanced concrete materials and the proposed models can be applied to predict the materials property.

2. Experimental program

2.1. Materials

In this study, several raw materials are used, including Portland cement CEM I 52.5 R (PC), densified micro-silica of Elkem Grade 920E D (mS), limestone powder (LP), fine silica sand (S), coarse basalt aggregate (BA), polycarboxylic ether (PCE) based superplasticizer (SP) and tap water (W). Fig. 1 shows the particle size distribution of raw materials. The detailed information about specific densities and oxide composition of the used materials are shown in Tables 1 and 2, respectively.

2.2. Mix design

The properties of TS-UHPC are mainly determined by two key aspects: grout and aggregate. In this study, three ultra-high performance grouts are designed with relatively low water-to-powder ratios, with different fine sand-to-powder ratios at 0, 0.5, and 1.0. The proportion of powders is optimized at 5% of micro-silica and 20% of limestone powder by mass of the total powder, based on our previous research [12]. The water content and superplasticizer dosage are adjusted to achieve a comparably desirable fluidity, with spread flow approximately between 35 cm and 40 cm by using a Hägermann cone [1]. The detailed recipes for the designed grouts are shown in Table 3.

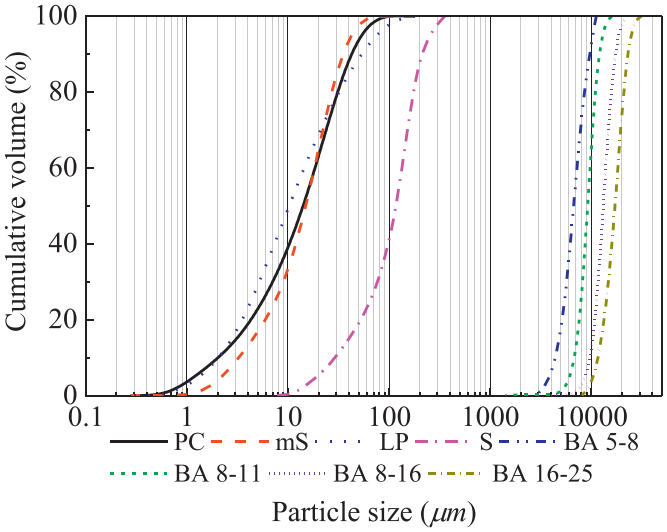

Fig. 1. The PSD of raw materials.

Four coarse basalt aggregates with different sizes are utilized to produce TS-UHPC, as shown in Fig. 2. To pre-estimate the ingredient consumption of designed TS-UHPC before concrete casting, the bulk densities of basalt aggregates are first measured in accordance with EN 1097-3 [26], shown in Table 1. Then the masses of ingredients can be calculated as,

$$m_{BA} = \rho_{bulk} \times 1m^3 \quad (1)$$

$$m_i = m_{i\_grout}\left(1 - \frac{\rho_{bulk}}{\rho_{specific}}\right) \quad (2)$$

where m_{BA} is the mass of basalt aggregates in TS-UHPC (kg/m^3). m_i and m_{i_grout} are the masses of other raw material i in TS-UHPC and the used grout (kg/m^3), respectively. ρ_{bulk} and $\rho_{specific}$ are the bulk and specific densities of used basalt aggregates (kg/m^3). The actual raw material consumptions for 1 cubic meter during the tests are shown in Table 4. The mix 1–4 contain grout of G2, and basalt aggregates of 5–8 mm, 8–11 mm, 8–16 mm and 16–25 mm, respectively. Mix 5–6 include basalt aggregates of 8–16 mm, and grout of G1 and G3, respectively. It should be noted that the volumes of coarse aggregates are around 55%, which is much higher than that in normal concrete.

2.3. Mixing and casting procedure

The coarse basalt aggregates are preplaced in a steel mould first. Then, the ultra-high performance grout is prepared following the procedure: drying mixing (PC + mS + LP + S) for 2 min, adding 80% water and mixing for 3 min, sequentially adding remaining water incorporated with SP and followed by mixing for about another 5 min. After that, the fresh ultra-high performance grout is poured into the preplaced coarse basalt aggregates. Several injecting methods can be found in literature, such as covering the top of moulds with a perforated plate and pumping grout into moulds from the bottom (need extra pumping device and energy) [27], pouring the grout from the top of aggregates by gravity effect (difficult to observe any possible honeycombed problem at bottom for finer aggregates) [22], injecting grout from bottom through a pipe by gravity effect (easy to adjust the injecting pressure by different height) [20], or even scatting-filling coarse aggregate process [28]. Using an injecting pipe by gravity effect is chosen in this paper by considering quality control, convenience of casting and economic benefit. The detail casting procedure for TS-UHPC is illustrated in Fig. 3(a). One example of the cross-section of hardened concretes (100 × 100 mm^2) by this casting procedure is

Table 1
Specific densities of raw materials.

Materials	PC	mS	LP	S	W	SP	BA 5–8	BA 8–11	BA 8–16	BA 16–25
Specific density (kg/m^3)	3150	2320	2710	2670	1000	1200	3050	2890	2710	3050
Bulk density (kg/m^3)	–	–	–	–	–	–	1715	1582	1514	1563

shown in Fig. 3(b), which presents very homogeneous distribution of coarse basalt aggregates and densified matrix.

2.4. Experimental and methods

2.4.1. Fresh behaviour

The fresh behaviour of grout is described by mini slump flow, mini V-funnel flow time and wet packing density. The mini slump flow and flow time are measured by a mini truncated conical cone without jolting and a mini V-funnel, respectively, in conformity with the EFNARC specification [29], at room temperature of about 20 ± 2 °C. The wet packing density ϕ is applied to reflect the compactness under the real wet condition, which is described by the solid concentration [30],

$$\phi = \sum_i^n \frac{r_i}{\rho_i} \frac{\rho}{(1 + w/s)} \quad (3)$$

where r_i and ρ_i are the mass fraction and density of solid material i. ρ is the fresh density of paste. w/s is the water-to-solid ratio.

2.4.2. Isothermal calorimetry

To research the hydration kinetics of the three different ultra-high performance grouts, an isothermal calorimeter is utilized to test the heat flow, at the temperature of 20 ° C (TAM Air, Thermometric). The fresh grouts are immediately filled into an ampoule and then put into the calorimeter. The heat flow is recorded continuously for approximately 3 days.

2.4.3. Thermal gravimetry

A Netzsch simultaneous analyser (model STA 449 C) is used to measure the thermal gravimetric (TG) and differential thermal gravimetric (DTG) curves of hardened grouts at the age of 56 days. The measurement is conducted at the heating rate of 10 °C/min, from 20 °C to 1000 °C under the flowing nitrogen environment. The samples are firstly ground and then the fineness is controlled by using a 63 μm sieve.

2.4.4. Mercury intrusion porosimetry

The pore structures of the hardened grouts are measured by mercury intrusion porosimetry (MIP, Micromeritics AutoPore IV). The inner parts of samples are crushed into small pieces of 2–4 mm after 56 days water curing. Dried specimens, around 1.5 g, are used for the analysis. The intrusion pressure changes from 0 to 227 MPa, with an Hg surface tension of 485 dynes/cm and contact angle of 130°.

2.4.5. Mechanical strength

The cubic specimens (50 × 50 × 50 mm^3) of grouts are produced for compressive strength test, based on EN 12390-3: 2009 [31]. The cubic specimens (100 × 100 × 100 mm^3) of TS-UHPC are cast for compressive and splitting tensile strength test, following EN 12390-3: 2009 [31] and EN 12390-6: 2009 [32], respectively. All the samples are covered with plastic film to keep moisture for 1 day. Then, the hardened specimens are demoulded and cured in water under temperature of 20 ± 2 °C, and then tested after desirable dates.

2.4.6. Scanning electron microscopy

Small pieces of dried hydrated samples after 56 days water curing are impregnated with an epoxy resin and polished down to 1 μm. The polished samples were examined in a scanning electron microscope (SEM, Bruker D2 Phaser) with an accelerating voltage of 15 kV.

2.4.7. Water permeable porosity

The water permeable porosity of the hardened grout and TS-UHPC are measured by using the vacuum-saturation technique [6]. The samples are cut from the cubic specimens in Section 2.4.5 after 91 days with a thickness of about 20 mm. The water permeable porosity φ (%) can be calculated as,

$$\varphi = \frac{m_s - m_d}{m_s - m_w} \times 100 \quad (4)$$

where m_s, m_d and m_w are the masses of sample measured in air after water saturation by vacuum condition, in air after oven drying, in water after water saturation by vacuum condition, respectively. The detailed testing procedure can be seen in [6], and the value stability of m_s and m_d is checked until reaching constant masses, respectively.

3. Results and discussion

3.1. Properties of grout

3.1.1. Fresh behaviour

The casting method and quality control of TS-UHPC are dependent on excellent fresh behaviour of ultra-high performance grout. The fresh behaviour of the three designed grouts is shown in Table 5. The mini slump flow ranges from 41 cm to 36 cm, while the mini V-funnel flow time changes from 5.5 s to 9.7 s, by adjusting the water content and SP dosage to meet the required self-compacting properties (slump flow of 24 to 26 cm and V-funnel time of 7 to 11 s) [29,33]. The fresh behaviour of the grouts is sufficient to be filled into the voids between aggregates, by checking the apparent and cross-section characters, as shown in Fig. 3 (b). It also should be pointed out that the mini slump flow above 35 cm is appropriate for ultra-high performance grout to fill the voids of aggregates in this study. The wet packing density calculated based on Eq. (3) continuously increases from 0.611 to 0.721, which means an improved compactness in fresh state for ultra-high performance grout with the addition of an appropriate fine sand content. The air content of the grouts determined based on [6] vary from 1.4% to 2.6%.

3.1.2. Hydration and pore structure

To understand the hydration and pore structure of the designed grouts, normalized heat flow, TG-mass loss and pore size distribution

Table 2
Oxide composition of powders.

Substance (%)	CaO	SiO_2	Al_2O_3	Fe_2O_3	K_2O	Na_2O	SO_3	MgO	TiO_2	MnO
PC	64.60	20.08	4.98	3.24	0.53	0.27	3.13	1.98	0.30	0.10
mS	0.90	93.06	–	2.06	1.15	0.63	1.28	0.70	–	0.07
LP	97.21	0.87	0.17	0.13	–	–	0.11	1.17	0.01	0.01

Table 3
Recipes of designed grouts.

Mix (Ga)	PC	mS	LP	S	water	SP	PC	mS	LP	S	water	SP
	Mass proportion						(kg/m^3)					
G1	0.75	0.05	0.20	0	0.200	1.3%	1378.0	91.9	367.5	0.0	367.5	23.9
G2	0.75	0.05	0.20	0.50	0.215	1.7%	1000.2	66.7	266.7	666.8	286.7	22.7
G3	0.75	0.05	0.20	1.00	0.240	2.0%	777.5	51.8	207.3	1036.6	248.8	20.7

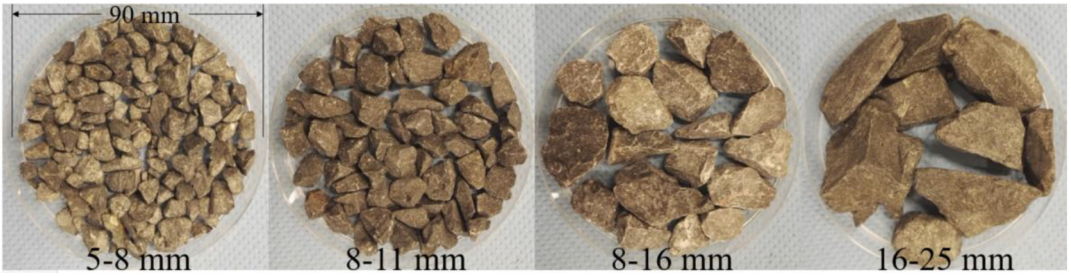

Fig. 2. The coarse basalt aggregates.

Table 4
Recipes of designed TS-UHPC (kg/m^3).

Mix no.	Note	PC	mS	LP	S	BA	water	SP	Density
1	G2A8	430.9	28.7	114.9	287.2	1715	123.5	9.8	2710
2	G2A11	450.8	30.1	120.2	300.5	1582	129.2	10.2	2623
3	G2A16	426.1	28.4	113.6	284.1	1514	122.1	9.7	2498
4	G2A25	478.9	31.9	127.7	319.3	1563	137.3	10.9	2669
5	G1A16	625.7	41.7	166.9	0.0	1514	166.9	10.8	2526
6	G3A16	341.5	22.8	91.1	455.3	1514	109.3	9.1	2543

Table 5
Fresh behaviour of grouts.

Mix	Flow (cm)	$T_{v\text{-funnel}}$ (s)	Fresh density (kg/m^3)	Wet packing density	Air content
G1	41	5.5	2197	0.611	1.4%
G2	38	9.2	2253	0.684	2.4%
G3	36	9.7	2281	0.721	2.6%

are measured. Fig. 4 shows the time-dependent normalized heat flow of ultra-high performance grouts with different sand contents, water amounts and PCE-type SP dosages. As seen from Table 3, the water proportion and SP dosage continuously increase with the increase of the sand content from 0 to 1.0 (sand-to-powder ratio), even though their absolute masses decrease. Compared to G1 without any sand, G2 (0.5) exhibits a shorter time to reach the peak of heat flow curve and releases more normalized heat, which is probably due to the nucleation effect of the very fine particles of sand that accelerate the hydration of binders. However, with further increasing the water-to-binder ratio and SP dosage, as shown in Table 3, G3 (1.0) shows a longer time to reach the peak, which indicates a larger retardation effect due to a higher PCE-type SP dosage and a higher water-to-binder ratio in UHPC system [1,34,35]. This retardation effect is dominant in the hydration of binders, instead of the acceleration effect by fine sand particles.

Fig. 5 presents the thermogravimetric results with TG and DTG curves. Three dominant peaks can be observed, which are respectively linked to the water loss from free water, C-S-H, ettringite and AFm dehydration (30–200 °C); decomposition of portlandite (CH) (400–500 °C); decarbonation of $CaCO_3$ (600–800 °C) [36,37]. All the three peaks tend to be weaker and sharper with the increased amount of fine sand, which indicates the dilution effect of fine sand on active

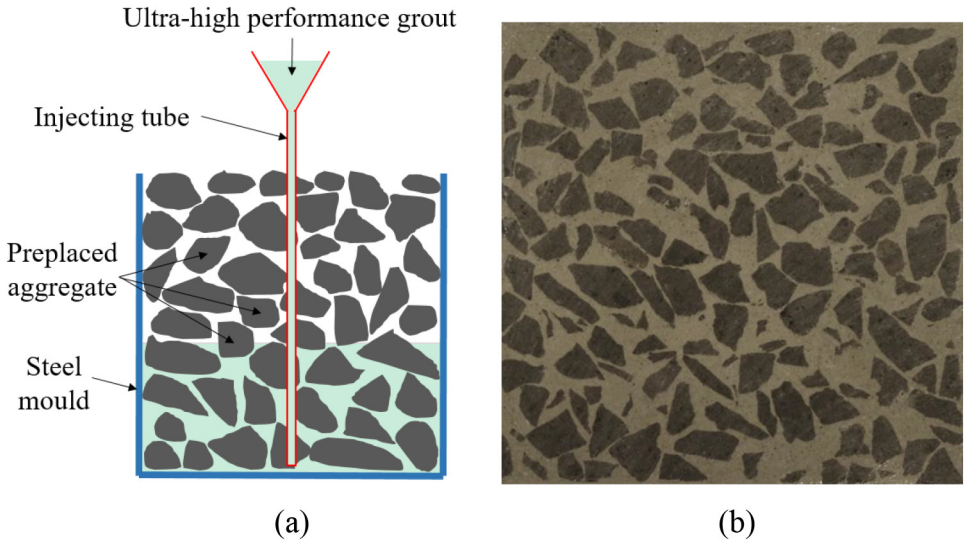

Fig. 3. (a) casting procedure and (b) cross-section of TS-UHPC.

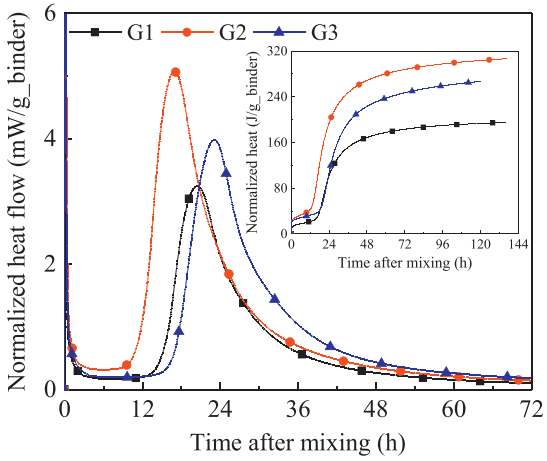

Fig. 4. Calorimetric results of grouts.

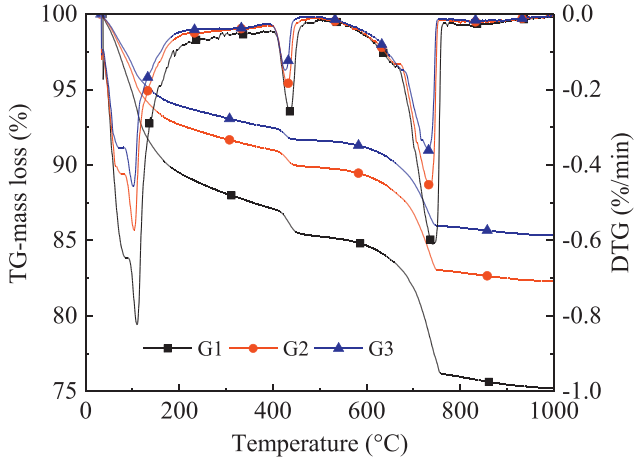

Fig. 5. Thermogravimetric results of grouts.

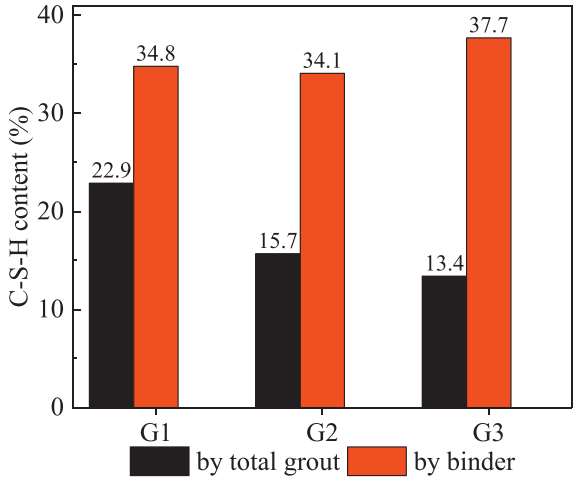

Fig. 6. C-S-H contents of gouts.

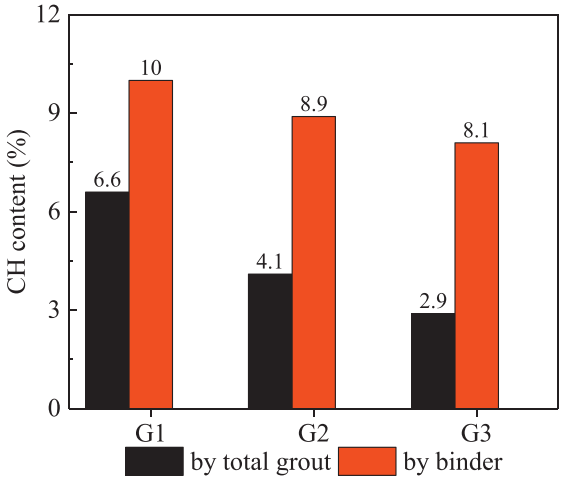

Fig. 7. CH contents of grouts.

binders. The contents of CH in designed grouts can be directly calculated from TG curves by,

$$\mathrm{CH}\,(\%) = \frac{M_{\mathrm{CH}}}{M_{\mathrm{H}}} \times \Delta m_{\mathrm{CH}}(\%) \tag{5}$$

where M_{CH} and M_{H} are the molar masses of calcium hydroxide and water, respectively. Δm_{CH} is the mass loss due to calcium hydroxide decomposition in percentage. Furthermore, the C-S-H contents can be estimated based on mass loss between 150 °C to 400 °C [38],

$$\mathrm{C\text{–}S\text{–}H}(\%) = \frac{M_{\mathrm{CSH}}}{2.1 M_{\mathrm{H}}} \times \Delta m_{\mathrm{CSH}}(\%) \tag{6}$$

where M_{CSH} is the molar mass of C-S-H gel. Δm_{CSH} is the mass loss corresponding to C-S-H dehydration in percentage from TG curve (150–400 °C). The water content in C-S-H gel has been extensively investigated, and varies depending on cement type, water-to-cement ratio, hydration degree, mineral addition, relative humidity and temperature, etc. [39–41], and the stoichiometric amount of water in this study is taken as 2.1 in Eq. (6), as suggested in [39]. The contents of C-S-H and CH are shown in Figs. 6 and 7, respectively. Even though the absolute C-S-H (by total grout) decreases with the increasing sand content, the C-S-H content by the mass of binder (PC + mS) keeps almost the same at around 34% from G1 to G2, and finally reaches up to 37.7% for G3. It indicates a higher hydration degree of active binder for G3 compared to G1, due to a higher water-to-binder ratio in G3. The higher hydration degree of G3 can also be directly observed by the amount of unreactive cement grains from the SEM observation that will be discussed in the following Section 3.3.1. G3 processing a higher hydration degree at a higher water-to-binder ratio should also generate more CH content by the mass of binder. However, a continuous decrease of CH content by the mass of binder is observed from G1 of 10% to G3 of 8.1%. It is probably attributed to a better pozzolanic effect of micro-silica in UHPC system with a higher water-to-binder ratio and consumes more CH to form C-S-H gel.

Fig. 8 shows the cumulative pore volume and differential pore size distribution of the grouts, which includes the pore size from 5 nm to 100 μm. It is clear that grout with a larger fine sand-to-powder ratio (up to 1.0 in this study) has lower cumulative pore volume, namely a lower porosity. The critical or threshold pore diameter (the peak on the pore size distribution curve in Fig. 8(b)), defined as the pore when achieving the highest rate of mercury intrusion and beginning to penetrate the interior of sample [37,42], decreases from around 26 nm of G1 to 21 nm of G2 with the increase of fine sand addition, and further keeps at 21 nm till G3. In this study, the pore size can be categorized into three parts as: (I) large pore more than 40 nm (air pore and partly capillary pore), (II) medium pore from around 20 nm to 40 nm (capillary pore), and (III) small pore from around 5 nm to 20 nm (partly gel pore and capillary pore [43]). The three grouts share comparable pore volumes from 40 nm to 100 nm, as shown in Fig. 8(a). While, with the addition of fine sand as filler, the grout of G2 (0.5), have a considerable decrease of the pores between 20 nm and 40 nm compared to that of G1, which can be attributed to the better compactness and reduced amount of the paste. As can be seen in Table 5, although G2 has a higher water-to-

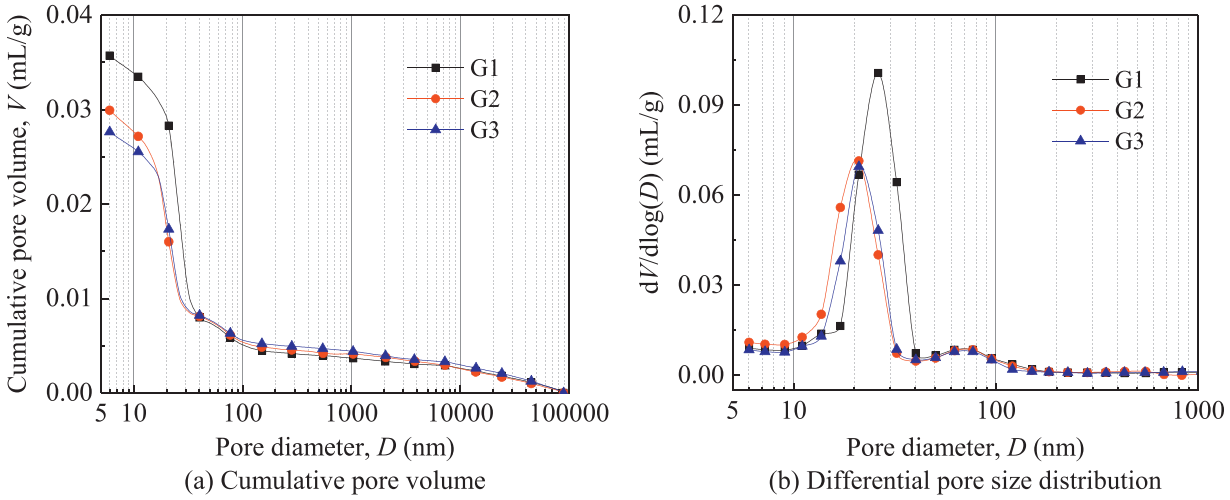

Fig. 8. Pore structure of grouts.

powder ratio that increases the capillary pores in the paste, G2 has a clearly lower amount of paste. Further addition of fine sand (G3) does not obviously increase the wet packing density, and cannot further improve the pore size distribution from 20 nm and 40 nm. G2 has a higher pore volume from 5 nm to 20 nm compared to G3, which can be explained by the relatively more C-S-H gel content in the grout (see Fig. 6). The G2 and G3 have more pores from 5 nm to 20 nm compared to G1, but less C-S-H gel phase (see Fig. 6), which indicates that more low-density and more porous C-S-H gels are preferably generated in G2 and G3 with higher water-to-powder ratios [43]. In overall, grout with a higher sand-to-powder ratio, 1.0 in this study, has a denser microstructure.

3.1.3. Strength development

Fig. 9 shows the compressive strength development of grouts. The early age strengths are very high, ranging between 66 and 100 MPa at 1 day, and then around 125 MPa at 7 days. The strength reaches between 142 MPa and 148 MPa at 28 days, and even higher at 91 days between 162 MPa and 173 MPa. These results confirm that ultra-high performance grouts can be successfully developed by applying the concept of UHPC, with both high early and later age strength. It could be used to design the TS-UHPC, and to predict the strength by that of grout (analysed in Section 3.3.3).

Grout with less fine sand processes higher early age strength before 7 days, which is due to higher amount of active binders and hydration product, as can be seen in Table 3 and Fig. 6. After a longer curing time, all the grouts reach comparable compressive strengths at 7 days. Later the grouts with more fine sand tend to surpass, e.g. 6.8% higher for G3 compared to G1. Two main factors contribute to those higher later compressive strengths, including better compactness (shown in Table 5) and relatively higher hydration degree of binders (analysed in Section 3.1.1). In overall, incorporating an appropriate amount of fine sand in ultra-high performance grout can improve its strength and reduce the binder consumption, which obviously contributes to sustainability development of advanced concrete materials.

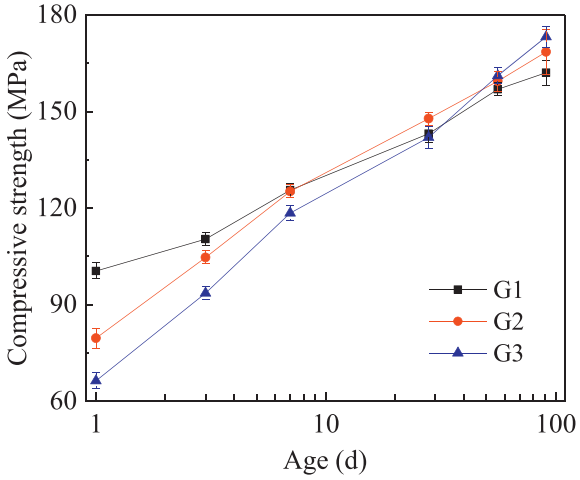

Fig. 9. Compressive strength of grouts.

3.2. Mechanical behaviour of TS-UHPC

Table 6 summarizes the compressive strength (σ_c) and splitting tensile strength (σ_t) of the designed TS-UHPC. The size effect of basalt aggregate, grout type effect, correlation between compressive and splitting tensile strength of TS-UHPC, and binder efficiency compared to normal TSC and UHPC will be discussed in the following sections.

3.2.1. Size effect of basalt aggregates

To analyse the size effect of coarse basalt aggregate, the mechanical strengths of TS-UHPC incorporated with G2 and different aggregate sizes are measured at 28 days, as shown in Fig. 10. It should be noted that currently most UHPCs are designed without applying any coarse aggregate to improve homogeneity and eliminate intrinsic weakness [2,3,5,44,45]. However, introduction of coarse aggregate has shown advantages, including decrease of powders, economic benefits [12], low shrinkage [28,46] and high impact resistance [47,48]. The utilized powder contents of TS-UHPC are very low compared to normal UHPC because the preplaced coarse basalt aggregates already occupy rather large volume (around 55%). Although the coarser aggregates are easily for grout to fill into the voids, the demanded powder contents are comparable for coarse aggregates with different sizes. Fig. 10 indicates a continuous decrease of both compressive and splitting tensile strength of TS-UHPC when increasing the maximum size of basalt aggregates, from 142.1 MPa to 121.8 MPa for compressive strength and 7.4 MPa to 6.5 MPa for splitting tensile strength. Because the volume of basalt aggregates is very similar, this reduction is mainly determined by the size effect of basalt aggregate. However, the reduction is not significant, approximately 14.3% and 12.2% respectively, with the maximum size from 8 mm to 25 mm. This limited decreasing tendency is in line with the conventional UHPC in our previous study [12]. The compressive damage pattern of the designed TS-UHPC usually shows an “explosive failure” as described in EN 12390–3: 2009 [31], which is similar to that of high strength concrete or plain UHPC.

Table 6
Strength of TS-UHPC (MPa).

Mix	Compressive strength σ_c						Splitting tensile strength σ_t					
	1d	3d	7d	28d	56d	91d	1d	3d	7d	28d	56d	91d
G2A8	–	–	–	142.1	–	–	–	–	–	7.4	–	–
G2A11	–	–	–	131.0	–	–	–	–	–	7.1	–	–
G2A16	80.5	105.3	114.1	116.2	124.0	140.1	4.0	5.9	6.3	6.6	6.9	7.5
G2A25	–	–	–	121.8	–	–	–	–	–	6.5	–	–
G1A16	87.4	109.5	111.3	113.0	118.1	127.6	4.5	5.3	5.6	5.9	6.1	6.6
G3A16	71.1	103.2	114.2	121.1	133.9	151.8	4.2	6.1	6.8	7.2	7.8	8.8

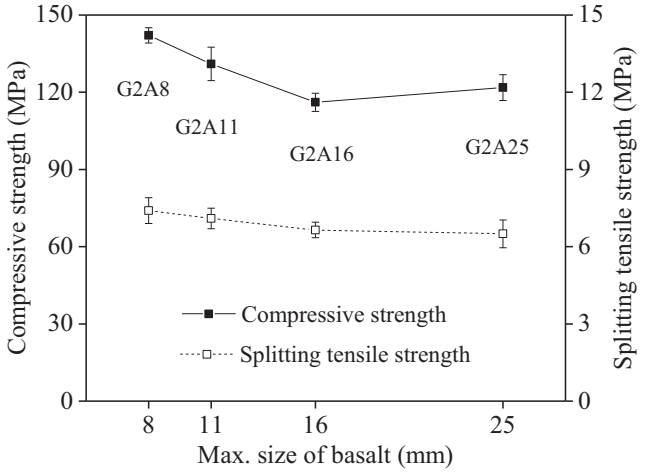

Fig. 10. Strength of TS-UHPC with different aggregate sizes at the age of 28 days.

3.2.2. Effect of grout type on strength development

Fig. 11 shows the strength development of TS-UHPC with different types of grouts at the maximum basalt size of 16 mm. The strength development of TS-UHPC follows the similar trend to that of ultra-high performance grout, namely smaller early strengths before 7 days and surpassed larger later strengths, with higher fine sand contents. The development rates of compressive and splitting tensile strength are not synchronized. TS-UHPC with more fine sand develops a faster splitting tensile strength, which indicates that splitting tensile strength is more positively sensitive to fine aggregates. The increase rate of tensile strength is approximately 33% from 6.6 MPa (G1A16) to 8.8 MPa (G3A16) at 91 days, while 19% for compressive strength from 127.6 MPa to 151.8 MPa.

3.2.3. Correlation between compressive and splitting tensile strength of TS-UHPC

For certain engineering applications, both compressive strength and tensile strength are of interest, such as the design of highway and airfield slabs, and cracking resistant component. Normally, a TSC processing a higher compressive strength has a larger splitting tensile strength. Several empirical equations have been established to present the correlation between the compressive strength ($\sigma_{c\_concrete}$) and splitting tensile strength ($\sigma_{t\_concrete}$) of conventional TSC, such as Abdelgader and Ben-Zeitun [49], Rajabi and Omidi-Moaf. [23], respectively, as,

$$\sigma_{t\_concrete} = 0.768 \cdot \sigma_{c\_concrete}^{0.441} \quad (7)$$

$$\sigma_{t\_concrete} = 0.638 \cdot \sigma_{c\_concrete}^{0.460} \quad (8)$$

Successful applications of those empirical equations have been confirmed by properties of conventional TSC with relatively low strength. The empirical formulas usually follow the type of $\sigma_{t\_concrete} = k \cdot \sigma_{c\_concrete}{}^{n}$, where k and n are coefficients. Values of n for normal concrete have been suggested below 0.75 by e.g. American Concrete Institute and Euro Code, which indicates that $\sigma_{t\_concrete}$-to-$\sigma_{c\_concrete}$ ratio decreases with an increase in $\sigma_{c\_concrete}$ [50]. However, those empirical predicting models are not appropriate for the TS-UHPC developed in this study, as shown in Fig. 12. Hence, a new model following the same format is proposed to describe the correlation between compressive strength and splitting tensile strength of TS-UHPC,

$$\sigma_{t\_concrete} = 0.029 \cdot \sigma_{c\_concrete}^{1.129} \ (R^2 = 0.81) \quad (9)$$

Fig. 12 shows a successful prediction on relationship between compressive and splitting tensile strength of TS-UHPC, where the R^2 value is 0.81. It can be seen that the experimental results of the

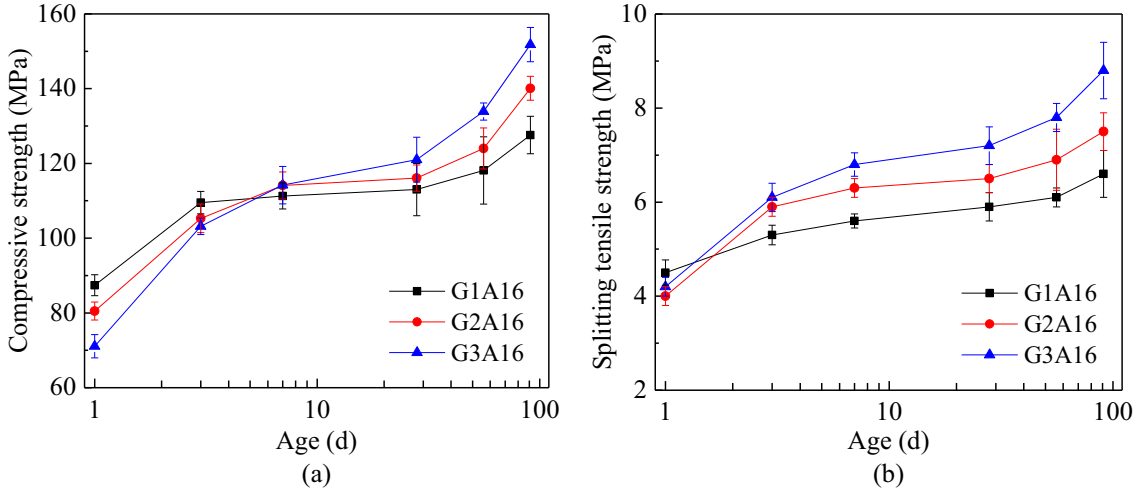

Fig. 11. Strength of TS-UHPC with different grouts.

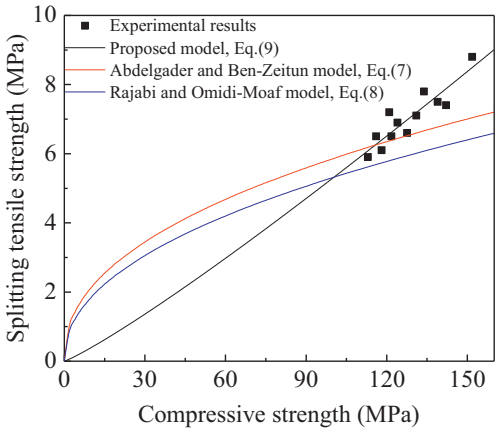

Fig. 12. Compressive versus splitting tensile strength of TS-UHPC.

designed TS-UHPC are usually above the empirical curves of Eqs. (7)–(8), especially when the compressive strength surpasses 120 MPa. The coefficient n is 1.129 (slightly larger than 1), which means that $\sigma_{t\_concrete}$-to-$\sigma_{c\_concrete}$ ratio slightly increases with an increase in $\sigma_{c\_concrete}$. It is concluded that the designed TS-UHPC has a higher $\sigma_{t\_concrete}$-to-$\sigma_{c\_concrete}$ ratio compared to the conventional TSC, indicating a wider engineering application potential thanks to the higher splitting tensile strength. The relatively higher $\sigma_{t\_concrete}$-to-$\sigma_{c\_concrete}$ ratio of TS-UHPC is probably attributed to the less shrinkage-induced micro-cracks due to very low binder utilization, and high intrinsic strength of basalt that provides aggregate bridging effect on tensile strength [51].

3.2.4. Binder efficiency

As can be seen in Table 4, the designed TS-UHPC has low binder consumption, ranging between 364 kg/m^3 and 667 kg/m^3, which is significantly lower compared to conventional UHPC (usually more than 900 kg/m^3) [8]. To further analyse the advantage of binder consumption and economic benefit of designed TS-UHPC, the binder efficiency X is applied as [13],

$$X = \sigma_c / m_{binder} \tag{10}$$

where X is binder efficiency (MPa·kg/m^3), σ_c is the compressive strength of TS-UHPC (MPa) after 28 days, in this study the binder efficiency after 91 days is also calculated. m_{binder} is the total mass of binders (kg/m^3), namely cement and micro-silica in this study.

Fig. 13 shows the binder efficiencies of designed TS-UHPC compared to other reported UHPC [3,13,52–55] and TSC [33] without fibre

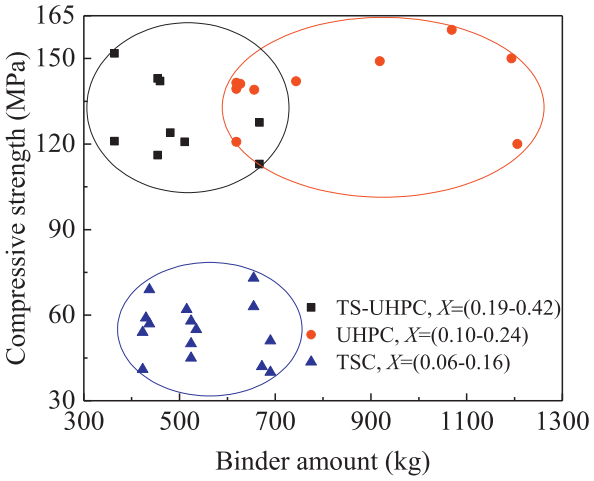

Fig. 13. Binder efficiency of the designed TS-UHPC.

under similar curing condition. It indicates that the designed TS-UHPC has a comparable compressive strength compared to other conventional UHPC in literatures, but very low binder amount (as low as 364 kg/m^3) and high binder efficiency (as high as 0.417). The designed TS-UHPC shows similar low or even lower binder consumption to normal TSC, approximately 350–700 kg/m^3, which is attributed to the high volume coarse aggregate consumption. However, the designed TS-UHPC can greatly overcome the relatively low strength of ordinary TSC (usually less than 70 MPa), and results in a much higher binder efficiency. The high binder efficiency of the designed TS-UHPC is attributed to very low water amount, pozzolanic addition and high-strength basalt aggregates. In overall, TS-UHPC is successfully developed combined with the advantages of both TSC and UHPC, namely very low binder amount, high binder efficiency, high volume of coarse aggregate, and ultra-high strength.

3.3. Compatibility between grout and aggregates

3.3.1. SEM observation

The mechanical property of the developed concrete is determined by the inherent property of the three phases: aggregate, grout and interfacial transition zone (ITZ). Normally, the ITZ is regarded as the weakest part of matrix and has a great influence on the mechanical and transport properties [56,57]. The ITZ is originally induced by water films around the aggregates and normally characterized by a higher porosity and larger pores compared to the paste, massive portlandite crystals precipitation, higher amount of porous ettringite and low-density C-S-H [56–58]. The ITZ of the designed TS-UHPC can be observed by SEM images, as shown in Fig. 14. Obviously, all the three ultra-high performance grouts can contribute to very tight ITZ with coarse basalt aggregate, compared to the ITZ in normal TSC [24]. The very dense ITZ is probably due to the very low water-to-binder ratios and excellent workability of the designed ultra-high performance grouts, which contribute to low porosities for both hardened ITZ and paste.

3.3.2. Porosity of grout, TS-UHPC and ITZ-induced

Besides the SEM observation, some quantitative methods are also used to directly analyse the ITZ property, e.g. statistical nano-indentation technique. However, they are usually complex and rely on expensive testing device [59,60]. In this study, a simple quantitative method, the water permeable porosity method, is utilized to further describe and analyse the ITZ. If the water permeable porosity of basalt aggregate is regarded as zero, the part of water permeable porosities in TS-UHPC caused by the ITZ can be deduced as,

$$\varphi_{ITZ-induced} = \varphi_{concrete} - \varphi_{grout} \times r_{grout} \tag{11}$$

where $\varphi_{ITZ-induced}$ is the ITZ-induced water permeable porosity; $\varphi_{concrete}$ and φ_{ITZ} are the water permeable porosities of TS-UHPC and grout, respectively; r_{grout} is the volume fraction of grout in TS-UHPC. The $\varphi_{ITZ-induced}$, $\varphi_{concrete}$ and φ_{grout} at 91 days are shown in Fig. 15, respectively. Both grout and TS-UHPC have a diminished water permeable porosities with the increasing content of fine sand, from 16.06% to 8.47% and 8.00% to 4.98%, respectively, which are in line with the trends to wet packing densities in Table 5 and mechanical strengths in Figs. 9 and 11. The water permeable porosities of TS-UHPC can be greatly improved in comparison with the corresponding grouts, due to the high content of aggregate utilization. However, the ITZ-induced water permeable porosities have a converse trend, increasing from G1A16 of 0.91% to G3A16 of 1.25%. The ITZ-induced porosity in the designed TS-UHPC (0.91%–1.25%) is much smaller compared to the normal concrete (1.7%–2.8%) with a comparable aggregate volume content (55%) [57], which demonstrates that the quality of the ITZ is very good. The relatively low ITZ-induced water permeable porosities are attributed to the designed ultra-high performance grout with superior fluidity to avoid entraining air void, relatively low water amount

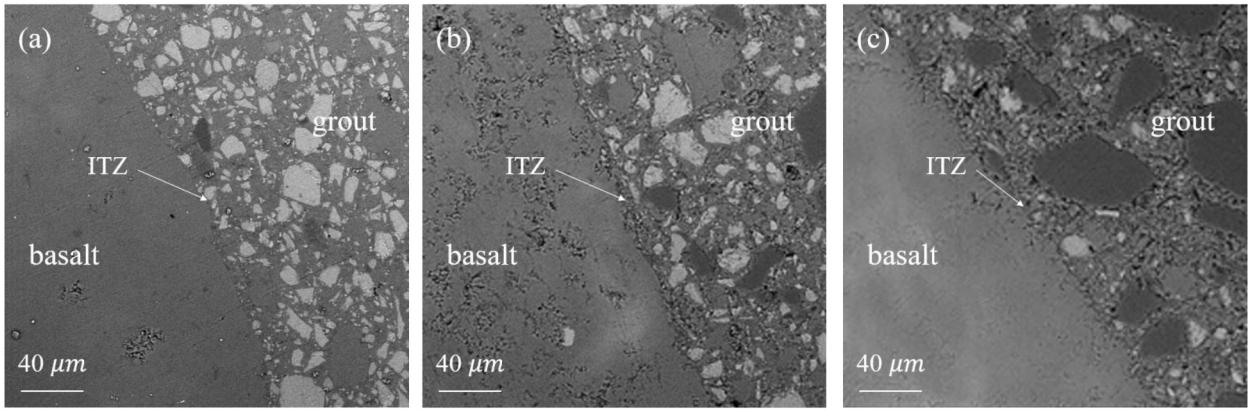

Fig. 14. SEM images of TS-UHPC, (a) G1A16, (b) G2A16, (c) G3A16.

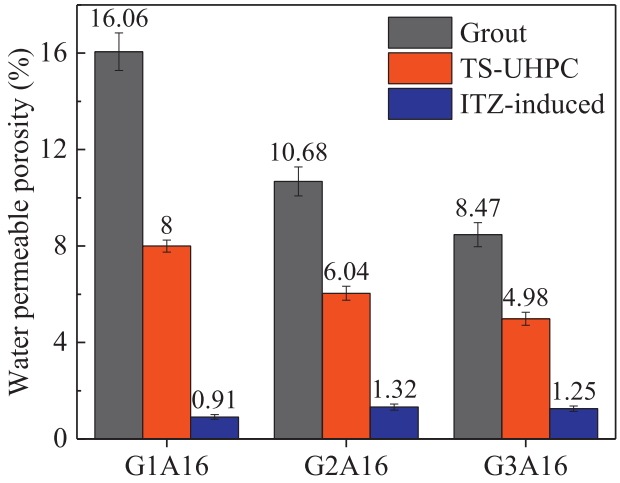

Fig. 15. Water-permeable porosity of grout, TS-UHPC and ITZ-induced.

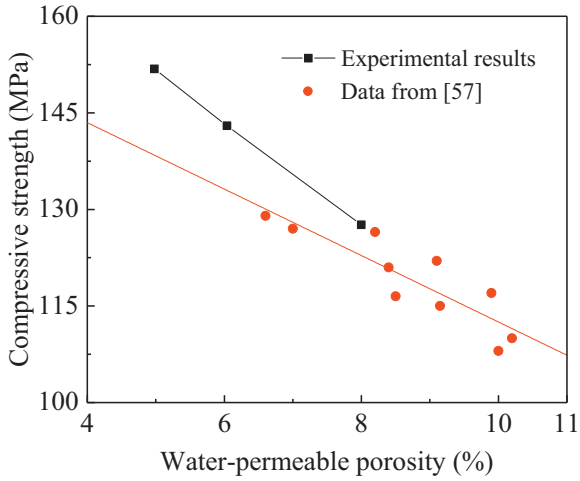

Fig. 16. Correlation between water-permeable porosity and compressive strength.

to reduce the water films around aggregates, addition of extra pozzolanic material (5% of micro silica in this paper) in grout to enhance the C-S-H generation.

To further analyse the influence of the ITZ-induced porosity (0.91%–1.32%) on mechanical properties of the designed TS-UHPC, the correlations between water-permeable porosity and compressive strength are compared with the existing results from literature [61], as shown in Fig. 16. It can be found that the compressive strength of TS-UHPC has almost a linear decrease with the increase of water-permeable porosity. Compared to the correlation in conventional UHPC, the designed TS-UHPC has a lower water-permeable porosity thanks to the high volume of coarse aggregate utilization. Furthermore, all the experimental results in this study are above the trend line of conventional UHPC, which means the water-permeable porosity has relatively lower negative effect on compressive strength of TS-UHPC compared to that of conventional UHPC. It also indicates the additional porosity caused by ITZ has rather limited negative effect on mechanical properties of TS-UHPC. Those phenomena are probably due to the high intrinsic strength or bonding ability of the basalt aggregates.

3.3.3. Predicting compressive strength of TS-UHPC

For a practical engineering application, it is wise to propose a model to predict the strength of TS-UHPC by a simple and reliable formula. Except for ITZ, the aggregate and grout are the other critical phases in concrete. Hence, the strength of aggregate and grout should be compatible and match with each other. The compressive strength of TS-UHPC can continuously increase when increasing the strength of grouts (seen in Fig. 9 and Table 6), which indicates that the limit of inherent strength of basalt aggregate is not reached in this study, with the maximum strength of grout at around 180 MPa. Some researchers reported that the strength of basalt is usually more than 200 MPa [47,62]. Hence, we can conclude that basalt aggregate is a good choice to produce TS-UHPC, which can match the strength of ultra-high performance grout. It has to be noted that the strength of TS-UHPC is always lower than the corresponding grout, due to the weakness of ITZ and strength concentration by point-to-point contact between aggregates [20].

The strengths of both grout (σ_{c_grout}) and TSC ($\sigma_{c\_concrete}$) depend on the similar key factors, including quality of mixing, binder amount, water content and fluidity [19], as well as fine sand addition and SP dosage. This dependence has been investigated by Abdelgader [19] as,

$$\sigma_{c\_concrete} = 6.70 + 0.42 \bullet \sigma_{c\_grout}^{1.07} \quad (12)$$

The empirical relationship offers a potential method to estimate TSC strength by primary grout strength. However, this empirical equation underestimates the compressive strength of the designed TS-UHPC, which is due to the utilized UHPC grouts and high-strength of basalt aggregates. Because the volumes of used grouts are in a very narrow range, around 45%, the compressive strength is mostly determined by the strength of grouts and the particle size of coarse aggregates. A new formula is proposed by considering both the effects of the used ultra-high performance cement grouts and the coarse aggregates size, applying the regression analysis of the present results to predict the compressive strength of TS-UHPC as,

$$\sigma_{c\_concrete} = (5.8 - 0.05D_{max}) \bullet \sigma_{c\_grout}^{0.64} \ (R^2 = 0.85) \quad (13)$$

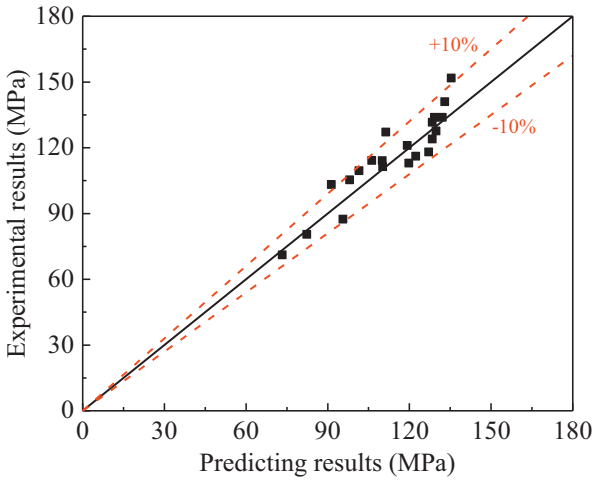

Fig. 17. Validation of predicting model.

It can be seen from Eq. (13) that the compressive strength of TS-UHPC is mainly dependent on the compressive strength of used grout, while the particle size (ranging from 5 mm to 25 mm) also has slightly adverse influence. As shown in Fig. 17, the experimental results fit to the predicting results very well, confirming the validity of the proposed model. Therefore, this model can be effectively applied to choose proper grout and aggregates to design TS-UHPC with a desired strength class. Nevertheless, further studies are needed to take different aggregate types into consideration.

4. Conclusions and future research suggestions

The present research develops the TS-UHPC as a novel building material with advantages of both TSC and UHPC, and investigates the properties of ultra-high performance grouts, corresponding TS-UHPC, and their compatibility. Based on the obtained results, the following conclusions can be drawn:

- TS-UHPC is a pioneering material concept with very low binder amount (down to 364 kg/m^3), high volume of coarse aggregate and high binder efficiency, according to two-stage (preplaced aggregate) method and high performance grout, with the compressive strength up to 151.8 MPa at the age of 91 days.
- When increasing the fine sand-to-powder ratio from 0 to 1.0, the grout tends to acquire a higher binder hydration degree, denser pore structure and compactness, increased later age strength and binder efficiency, and comparable fluidity.
- Coarser basalt aggregate tends to slightly lower the compressive and splitting tensile strength, around 14.3% and 12.2% reduction with the maximum size from 8 mm to 25 mm, respectively. The basalt aggregates with maximum size of 25 mm are suggested in TS-UHPC, due to the easier and faster grout injection during casting process, even though it needs slightly higher binder content and lower strength.
- The compatibility between grout and aggregate is analysed based on ITZ and correlation between the strength of grout and TS-UHPC. The designed TS-UHPC has an excellent ITZ quality, with low ITZ-induced porosity around 0.91%–1.32% compared to 1.7%–2.8% in normal concrete.
- New formulas are proposed to describe the relationship between the compressive and splitting tensile strength of TS-UHPC designed by ultra-high performance grouts and basalt aggregates, and to predict the compressive strength of TS-UHPC by the applied grout's strength and aggregates' size. The compressive of TS-UHPC is mainly determined by the used grout, while the aggregate size also has slightly adverse influence.

TS-UHPC is a newly developed ultra-low binder ultra-high performance concrete concept with widely potential application, e.g. impact resistant, underwater, massive, repaired, heavyweight, low-shrinkage concrete. Many key parameters and properties remain to be explored. Different types of coarse aggregates, ultra-high performance grout with optimal water and sand content, introduction of steel fibres are suggested to future research on mix design. Properties, such as impact resistance under bullet or projectile impact, shrinkage, abrasion resistance, thermo-mechanical behaviour of mass concrete can be scope for future study by both experimental and mesoscale modelling analysis.

Acknowledgements

This research was funded by the China Scholarship Council and Eindhoven University of Technology. Thanks are given to Mr. Gang Liu for his help with experiments.

References

[1] P.P. Li, Q.L. Yu, H.J.H. Brouwers, Effect of PCE-type superplasticizer on early-age behaviour of ultra-high performance concrete (UHPC), Constr. Build. Mater. 153 (2017) 740–750.
[2] D.Y. Yoo, N. Banthia, Mechanical properties of ultra-high-performance fiber-reinforced concrete: a review, Cem. Concr. Compos. 73 (2016) 267–280.
[3] R. Yu, L. van Beers, P. Spiesz, H.J.H. Brouwers, Impact resistance of a sustainable ultra-high performance fibre reinforced concrete (UHPFRC) under pendulum impact loadings, Constr. Build. Mater. 107 (2016) 203–215.
[4] W. Wang, J. Liu, F. Agostini, C.A. Davy, F. Skoczylas, D. Corvez, Durability of an ultra high performance fiber reinforced concrete (UHPFRC) under progressive aging, Cem. Concr. Res. 55 (2014) 1–13.
[5] P. Richard, M. Cheyrezy, Composition of reactive powder concretes, Cem. Concr. Res. 25 (1995) 1501–1511.
[6] R. Yu, P. Spiesz, H.J.H. Brouwers, Effect of nano-silica on the hydration and microstructure development of ultra-high performance concrete (UHPC) with a low binder amount, Constr. Build. Mater. 65 (2014) 140–150.
[7] C. Shi, D. Wang, L. Wu, Z. Wu, The hydration and microstructure of ultra high-strength concrete with cement–silica fume–slag binder, Cem. Concr. Compos. 61 (2015) 44–52.
[8] T. Stengel, P. Schießl, Life Cycle Assessment (LCA) of Ultra High Performance Concrete (UHPC) Structures, Woodhead Publishing Limited, 2014.
[9] J. Ma, M. Orgass, F. Dehn, D. Schmidt, N.V. Tue, Comparative investigations on ultra-high performance concrete with or without coarse aggregates, Proc Int Symp Ultra High Perform Concr Kassel, 2004, pp. 205–212.
[10] C. Jiang, Y.F. Wu, J.F. Jiang, Effect of aggregate size on stress-strain behavior of concrete confined by fiber composites, Compos. Struct. 168 (2017) 851–862.
[11] M.H. Zhang, V.P.W. Shim, G. Lu, C.W. Chew, Resistance of high-strength concrete to projectile impact, Int J Impact Eng 31 (2005) 825–841.
[12] P.P. Li, Q.L. Yu, H.J.H. Brouwers, Effect of coarse basalt aggregates on the properties of ultra-high performance concrete (UHPC), Constr. Build. Mater. 170 (2018) 649–659.
[13] P.P. Li, Q.L. Yu, Responses and post-impact properties of ultra-high performance fibre reinforced concrete under pendulum impact, Compos. Struct. 208 (2019) 806–815.
[14] S. Pyo, S. Yihune, H. Kim, Abrasion resistance of ultra high performance concrete incorporating coarser aggregate, Constr. Build. Mater. 165 (2018) 11–16.
[15] S. Pyo, H.K. Kim, B.Y. Lee, Effects of coarser fine aggregate on tensile properties of ultra high performance concrete, Cem. Concr. Compos. 84 (2017) 28–35.
[16] J. Liu, F. Han, G. Cui, Q. Zhang, J. Lv, L. Zhang, et al., Combined effect of coarse aggregate and fiber on tensile behavior of ultra-high performance concrete, Constr. Build. Mater. 121 (2016) 310–318.
[17] H. Wu, Q. Fang, X.W. Chen, Z.M. Gong, J.Z. Liu, Projectile penetration of ultra-high performance cement based composites at 510–1320 m/s, Constr. Build. Mater. 74 (2015) 188–200.
[18] H. Wu, Q. Fang, J. Gong, J.Z. Liu, J.H. Zhang, Z.M. Gong, Projectile impact resistance of corundum aggregated UHP-SFRC, Int J Impact Eng 84 (2015) 38–53.
[19] H.S. Abdelgader, How to design concrete produced by a two-stage concreting method, Cem. Concr. Res. 29 (1999) 331–337.
[20] M.F. Najjar, A.M. Soliman, M.L. Nehdi, Critical overview of two-stage concrete: properties and applications, Constr. Build. Mater. 62 (2014) 47–58.
[21] H.S. Abdelgader, J. Górski, Stress-strain relations and modulus of elasticity of two-stage concrete, J. Mater. Civ. Eng. 15 (2003) 329–334.
[22] M.L. Nehdi, M.F. Najjar, A.M. Soliman, T.M. Azabi, Novel steel fibre-reinforced preplaced aggregate concrete with superior mechanical performance, Cem. Concr. Compos. 82 (2017) 242–251.
[23] A.M. Rajabi, F. Omidi Moaf, Simple empirical formula to estimate the main geo-mechanical parameters of preplaced aggregate concrete and conventional concrete, Constr. Build. Mater. 146 (2017) 485–492.
[24] M.F. Najjar, A.M. Soliman, M.L. Nehdi, Two-stage concrete made with single, binary and ternary binders, Mater. Struct. 49 (2014) 317–327.

[25] M.F. Najjar, A.M. Soliman, M.L. Nehdi, Grouts incorporating supplementary cementitious materials for two-stage concrete, J. Mater. Civ. Eng. 29 (2017) 1–9.
[26] EN-1097-3, Tests for mechanical and physical properties of aggregates - part 3: determination of loose bulk density and voids, Br Stand Institution-BSI CEN Eur Comm Stand, 1998.
[27] M. Coo, T. Pheeraphan, Effect of sand, fly ash and limestone powder on preplaced aggregate concrete mechanical properties and reinforced beam shear capacity, Constr. Build. Mater. 120 (2016) 581–592.
[28] W. Shen, R. Dong, J. Li, M. Zhou, W. Ma, J. Zha, Experimental investigation on aggregate interlocking concrete prepared with scattering-filling coarse aggregate process, Constr. Build. Mater. 24 (2010) 2312–2316.
[29] EFNARC, Specification and guidelines for self-compacting concrete, Rep from EFNARC 44 (2002) 32.
[30] L.G. Li, A.K.H. Kwan, Packing density of concrete mix under dry and wet conditions, Powder Technol. 253 (2014) 514–521.
[31] EN 12390-3. Testing hardened concrete - part 3: Compressive strength of test specimens. Br Stand Institution-BSI CEN Eur Comm Stand 2009.
[32] EN 12390-6, Testing hardened concrete - part 6: Tensile splitting strength of test specimens, Br Stand Institution-BSI CEN Eur Comm Stand, 2009.
[33] M. Coo, T. Pheeraphan, Effect of sand, fly ash, and coarse aggregate gradation on preplaced aggregate concrete studied through factorial design, Constr. Build. Mater. 93 (2015) 812–821.
[34] Y. Zhang, X. Kong, Correlations of the dispersing capability of NSF and PCE types of superplasticizer and their impacts on cement hydration with the adsorption in fresh cement pastes, Cem. Concr. Res. 69 (2015) 1–9.
[35] Y.R. Zhang, X.M. Kong, Z.B. Lu, Z.C. Lu, S.S. Hou, Effects of the charge characteristics of polycarboxylate superplasticizers on the adsorption and the retardation in cement pastes, Cem. Concr. Res. 67 (2015) 184–196.
[36] Z. Wu, C. Shi, K.H. Khayat, Influence of silica fume content on microstructure development and bond to steel fiber in ultra-high strength cement-based materials (UHSC), Cem. Concr. Compos. 71 (2016) 97–109.
[37] W. Huang, H. Kazemi-Kamyab, W. Sun, K. Scrivener, Effect of cement substitution by limestone on the hydration and microstructural development of ultra-high performance concrete (UHPC), Cem. Concr. Compos. 77 (2017) 86–101.
[38] J. Jain, N. Neithalath, Analysis of calcium leaching behavior of plain and modified cement pastes in pure water, Cem. Concr. Compos. 31 (2009) 176–185.
[39] T. HFW, Cement Chemistry, 2nd ed., Thomas Telford, London, 1997.
[40] B. Lothenbach, K. Scrivener, R.D. Hooton, Supplementary cementitious materials, Cem. Concr. Res. 41 (2011) 1244–1256.
[41] J.E. Rossen, B. Lothenbach, K.L. Scrivener, Composition of C-S-H in pastes with increasing levels of silica fume addition, Cem. Concr. Res. 75 (2015) 14–22.
[42] R.A. Cook, K.C. Hover, Mercury porosimetry of hardened cement pastes, Cem. Concr. Res. 29 (1999) 933–943.
[43] J. Yajun, J.H. Cahyadi, Effects of densified silica fume on microstructure and compressive strength of blended cement pastes, Cem. Concr. Res. 33 (2003) 1543–1548.
[44] K. Habel, M. Viviani, E. Denarié, E. Brühwiler, Development of the mechanical properties of an ultra-high performance fiber reinforced concrete (UHPFRC), Cem. Concr. Res. 36 (2006) 1362–1370.
[45] C. Wang, C. Yang, F. Liu, C. Wan, X. Pu, Preparation of ultra-high performance concrete with common technology and materials, Cem. Concr. Compos. 34 (2012) 538–544.
[46] H.S. Abdelgader, A.A. Elgalhud, Effect of grout proportions on strength of two-stage concrete, Struct. Concr. 9 (2008) 163–170.
[47] Y. Peng, H. Wu, Q. Fang, J.Z. Liu, Z.M. Gong, Impact resistance of basalt aggregated UHP-SFRC/fabric composite panel against small caliber arm, Int J Impact Eng 88 (2016) 201–213.
[48] Y.S. Tai, S. El-Tawil, T.H. Chung, Performance of deformed steel fibers embedded in ultra-high performance concrete subjected to various pullout rates, Cem. Concr. Res. 89 (2016) 1–13.
[49] H.S. Abdelgader, A.E. Ben-Zeitun, Tensile strength of two-stage concrete measured by double-punch and split tests, Global Construction. Role of Concrete in Nuclear Facilities. Proceedings of International Conference, University of Dundee, Scotland, UK, 2005, pp. 43–50.
[50] A.M. Neville, Properties of Concrete, 4 edition, Prentice Hall, 2002.
[51] J. Zhang, C.K.Y. Leung, Y.N. Cheung, Flexural performance of layered ECC-concrete composite beam, Compos. Sci. Technol. 66 (2006) 1501–1512.
[52] R. Yu, Development of Sustainable Protective Ultra-High Performance Fibre Reinforced Concrete (UHPFRC), PhD thesis Eindhoven Universtiy of Technology, Eindhoven, the Netherland, 2015.
[53] A.M.T. Hassan, S.W. Jones, G.H. Mahmud, Experimental test methods to determine the uniaxial tensile and compressive behaviour of ultra high performance fibre reinforced concrete (UHPFRC), Constr. Build. Mater. 37 (2012) 874–882.
[54] S.L. Yang, S.G. Millard, M.N. Soutsos, S.J. Barnett, T.T. Le, Influence of aggregate and curing regime on the mechanical properties of ultra-high performance fibre reinforced concrete (UHPFRC), Constr. Build. Mater. 23 (2009) 2291–2298.
[55] R.D. Toledo Filho, E.A.B. Koenders, S. Formagini, E.M.R. Fairbairn, Performance assessment of ultra high performance fiber reinforced cementitious composites in view of sustainability, Mater. Des. 36 (2012) 880–888.
[56] M. Nili, A. Ehsani, Investigating the effect of the cement paste and transition zone on strength development of concrete containing nanosilica and silica fume, Mater. Des. 75 (2015) 174–183.
[57] K. Wu, H. Shi, L. Xu, G. Ye, G. De Schutter, Microstructural characterization of ITZ in blended cement concretes and its relation to transport properties, Cem. Concr. Res. 79 (2016) 243–256.
[58] A. Bentur, M.D. Cohen, Effect of condensed silica fume on the microstructure of the interfacial zone in Portland cement mortars, J. Am. Ceram. Soc. 70 (1987) 738–743.
[59] S. Erdem, A.R. Dawson, N.H. Thom, Influence of the micro- and nanoscale local mechanical properties of the interfacial transition zone on impact behavior of concrete made with different aggregates, Cem. Concr. Res. 42 (2012) 447–458.
[60] X.H. Wang, S. Jacobsen, J.Y. He, Z.L. Zhang, S.F. Lee, H.L. Lein, Application of nanoindentation testing to study of the interfacial transition zone in steel fiber reinforced mortar, Cem. Concr. Res. 39 (2009) 701–715.
[61] R. Yu, P. Spiesz, H.J.H. Brouwers, Development of an eco-friendly ultra-high performance concrete (UHPC) with efficient cement and mineral admixtures uses, Cem. Concr. Compos. 55 (2015) 383–394.
[62] R.A. Schultz, Comparative rock mass strengths of basalt and tuff and some planetological implications, 25th Lunar Planet. Sci. Conf., Houston, 1994, pp. 1217–1218.